

# **Aerosol Science and Technology**



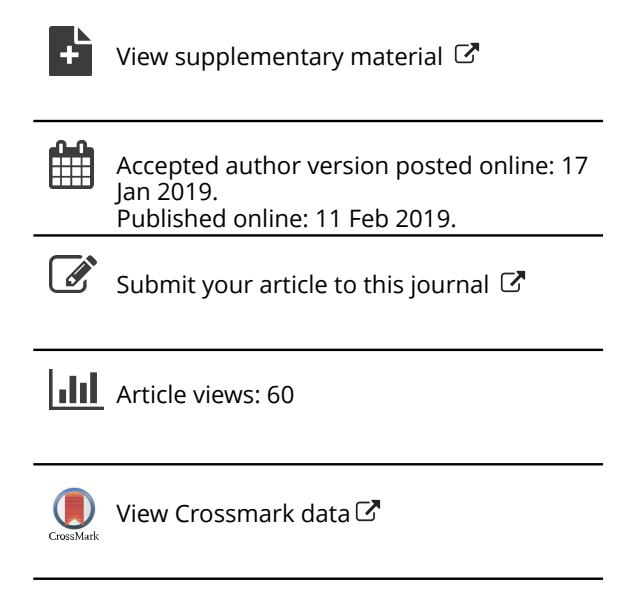
ISSN: 0278-6826 (Print) 1521-7388 (Online) Journal homepage: https://www.tandfonline.com/loi/uast20

# Growth of Aitken mode ammonium sulfate particles by $\alpha$ -pinene ozonolysis

Justin M. Krasnomowitz, Michael J. Apsokardu, Christopher M. Stangl, Lee Tiszenkel, Qi Ouyang, Shanhu Lee & Murray V. Johnston

To cite this article: Justin M. Krasnomowitz, Michael J. Apsokardu, Christopher M. Stangl, Lee Tiszenkel, Qi Ouyang, Shanhu Lee & Murray V. Johnston (2019): Growth of Aitken mode ammonium sulfate particles by  $\alpha$ -pinene ozonolysis, Aerosol Science and Technology, DOI: 10.1080/02786826.2019.1568381

To link to this article: <a href="https://doi.org/10.1080/02786826.2019.1568381">https://doi.org/10.1080/02786826.2019.1568381</a>









# Growth of Aitken mode ammonium sulfate particles by $\alpha$ -pinene ozonolysis

Justin M. Krasnomowitz<sup>a</sup> , Michael J. Apsokardu<sup>a</sup> , Christopher M. Stangl<sup>a</sup> , Lee Tiszenkel<sup>b</sup> , Qi Ouyang<sup>b</sup> , Shanhu Lee<sup>b,c</sup> , and Murray V. Johnston<sup>a</sup>

<sup>a</sup>Department of Chemistry and Biochemistry, University of Delaware, Newark, Delaware, USA; <sup>b</sup>Department of Atmospheric Science, The University of Alabama in Huntsville, Huntsville, Alabama, USA; <sup>c</sup>Department of Environmental Science and Engineering, Fudan University, Shanghai, China

### **ABSTRACT**

The fraction of Aitken mode particles that grow sufficiently large to act as cloud condensation nuclei is an important factor in understanding the climate impact of atmospheric particles. Elucidating the rate of particle growth in this size range requires a detailed understanding of the mechanisms by which these particles grow. Here, a flow tube reactor is described, characterized and then used to study growth of ammonium sulfate seed particles in the Aitken mode size range by  $\alpha$ -pinene ozonolysis under dry conditions (10% RH). When size-selected particles starting at 40, 60, or 80 nm diameter were exposed to  $\alpha$ -pinene (11 ppbv) and ozone (five separate mixing ratios between 30 and 250 ppbv), particle growth was found to depend on the amount of  $\alpha$ -pinene reacted and the condensation sink, but not directly dependent on the initial seed particle diameter. The observed dependencies are consistent with a condensational growth mechanism, which is not surprising since the dry conditions of the experiment minimized the probability of multiphase chemistry within the seed particles. Combining the measured particle growth with a kinetic model gave a molar yield of 13% for condensable organic molecules produced by the ozonolysis reaction. This value is somewhat higher than previously reported molar yields of highly oxidized molecules (HOMs) measured in the gas phase with chemical ionization mass spectrometry, which are in the 3-7% range. The relationship between molar yields determined from gas phase and particle phase measurements is discussed.

### **ARTICLE HISTORY**

Received 12 June 2018 Accepted 23 December 2018

#### **EDITOR**

Paul Ziemann

# 1. Introduction

Aitken mode particles span a size range of about 10-100 nm in diameter and can represent the largest number concentration of particles in ambient air (Komppula et al. 2003). Particles in this mode have potential to impact climate as they grow in size and are able to be activated as cloud condensation nuclei (CCN; Lihavainen et al. 2003; Komppula et al. 2005). In particular, the fraction of particles that are activated as CCN increase substantially with increasing particle diameter in the 50-100 nm size range (Dusek et al. 2006; Komppula et al. 2005). For this reason, a thorough understanding of the chemical processes behind Aitken mode particle growth is needed so that growth rates in the atmosphere can be accurately predicted along with their climate impact. The goal of this work is to study the mechanism and quantify the

amount of growth of ammonium sulfate seed particles in the Aitken mode size range by  $\alpha$ -pinene ozonolysis.

A substantial portion of ambient particle growth occurs by formation of secondary organic aerosol (SOA), and atmospheric models have a difficult time accurately predicting its contribution to aerosol mass loading (Donahue et al. 2012; Hallquist et al. 2009). Oxidation of biogenic volatile organic compounds (BVOCs) leads to the formation of products over a wide range of volatilities (Donahue et al. 2012; Jimenez et al. 2009). One such BVOC, α-pinene, accounts for half of total monoterpene emissions (Pathak et al. 2007) and is the precursor studied in this work. Reaction of BVOCs with ozone or OH produce highly oxidized products in the gas phase that are nonvolatile enough to nucleate and grow particles (Kulmala et al. 2013; Paasonen et al. 2013; Ehn et al. 2012; Riipinen et al. 2011). Most of these products are

CONTACT Murray V. Johnston myj@udel.edu Department of Chemistry and Biochemistry, University of Delaware, 102 Lammot Dupont Laboratory, Newark, DF 19716

Color versions of one or more of the figures in the article can be found online at www.tandfonline.com/uast.

Supplemental data for this article is available online at on the publisher's website.

**Table 1.** Molar yield of condensable molecules from  $\alpha$ -pinene ozonolysis.

Study	<b>Experimental conditions</b>	Molar yield (%)	Measurement approach
Ehn et al. (2014)	2 ppbv αP, 170 ppbv O <sub>3</sub> 289 K, 63% RH	7 (±3.5)	Determined from signal intensities of gas-phase species detected by NO <sub>3</sub> <sup>-</sup> Cl-APi-TOF; measurements under predict growth of 5–50 nm particles; reaction performed in a high volume chamber
Jokinen et al. (2015)	0.1–175 ppbv $\alpha$ P, 23 ppbv O $_3$ 293 K, 25% RH	3.4 (+3.4/-1.7)	Determined from signal intensities of gas-phase species detected by NO <sub>3</sub> <sup>-</sup> CI-APi-TOF; reaction performed in a flow tube
Kirkby et al. (2016)	333 pptv $\alpha$ P, 33 ppbv $O_3$ 278 K, 38% RH	2.9 (+5.2/-1.3)	Determined from signal intensities of gas-phase species detected by NO <sub>3</sub> CI-APi-TOF; reaction performed in a high volume chamber
Sarnela et al. (2018)	333 pptv $\alpha$ P, 33 ppbv $O_3$ 278 K, 38% RH	3.5–6.5	Determined from signal intensities of gas-phase species detected by NO <sub>3</sub> <sup>-</sup> Cl-APi-TOF; reaction performed in a high volume chamber
Krasnomowitz et al. (this work)	11 ppbv $\alpha$ P, 30–250 ppbv O $_3$ 297 K, 10% RH	13 (±1)	Determined from a kinetic model fit of measured diameter growth of 40–80 nm dia. seed par- ticles; reaction performed in a flow tube

formed through an autoxidation mechanism (Jokinen et al. 2015; Ehn et al. 2014; Rissanen et al. 2014; Crounse et al. 2013).

Determining particle growth rates from BVOC oxidation requires knowledge of the yield of molecular products that are nonvolatile enough to grow particles at their condensation rates. The effective saturation vapor pressure increases with increasing radius-ofcurvature of the gas-particle interface (i.e., Kelvin effect). This effect becomes substantial for particles in the low nanometer size range, meaning that some compounds which grow larger Aitken mode particles at the condensation rate may not efficiently grow smaller nucleation mode particles. The definitions of terms in the literature used to describe nonvolatile oxidation products have evolved over time (Tröstl et al. 2016; Ehn et al. 2014; Riccobono et al. 2014). Tröstl et al. (2016) proposed that highly oxidized molecules (HOMs) be defined as the full range of gasphase species detected by nitrate ion (NO<sub>3</sub><sup>-</sup>) chemical ionization in an atmospheric pressure interface timeof-flight mass spectrometer (CI-APi-TOF), whereas extremely low volatility organic compounds (ELVOCs) are the subset of detected species that are expected to have low enough vapor pressures to nucleate and condensationally grow particles in the low nanometer size range (Ehn et al. 2014). To make this distinction, Tröstl et al. (2016) used molecular formulas obtained with accurate mass measurements to calculate the corresponding saturation vapor pressures (C\* in units of μg/m³), based on the volatility based set (VBS, Donahue et al. 2011).

Yields for HOM formation from  $\alpha$ -pinene ozonolysis were first reported by Ehn et al. (2014) based on gas phase measurements of α-pinene oxidation products by NO<sub>3</sub> CI-APi-TOF. They reported a molar yield of 7% per precursor molecule that reacted with ozone, corresponding to a mass yield of 14% based on the assigned ion molecular formulas. These measurements were performed at 289 K and 63% RH using a flow-through chamber having a residence time of  $\sim$ 45 min. Uncertainties were estimated to be  $\pm$ 50% of the reported values. Using similar gas phase measurements, Jokinen et al. (2015) reported a HOM yield for α-pinene ozonolysis of 3.4% with an uncertainty of 1.7-6.8% for experiments performed at 293 K and 25% RH using a fast flow tube reactor with a 40 s residence time. Since then, other studies using NO<sub>3</sub><sup>-</sup> CI-APi-TOF have reported HOM yields in the 3-6% range (Kirkby et al. 2016; Sarnela et al. 2018). While all of these reported yields are based on gas phase measurements with NO<sub>3</sub><sup>-</sup> chemical ionization, they do differ slightly in the subset of detected ions used to calculate the yield and the experimental conditions studied, which may contribute to the range of values reported. Table 1 summarizes these measurements and the experimental conditions under which they were performed.

Three factors can affect the prediction of HOM yields from gas phase measurements. First, the definition of HOMs is based on a specific set of ions detected with chemical ionization, which may or may not include all relevant molecular species. Second, particle size-dependent phenomena such as the Kelvin effect on molecular volatility must be inferred from molecular formulas when considering which subset of detected ions to include in the yield calculation. Third, they do not take into account the possibility of heterogeneous chemical reactions that may add to the particle growth rate (Apsokardu and Johnston 2018). Measured particle growth rates tend to be underestimated by CI-APi-TOF measurements, e.g., see Figures

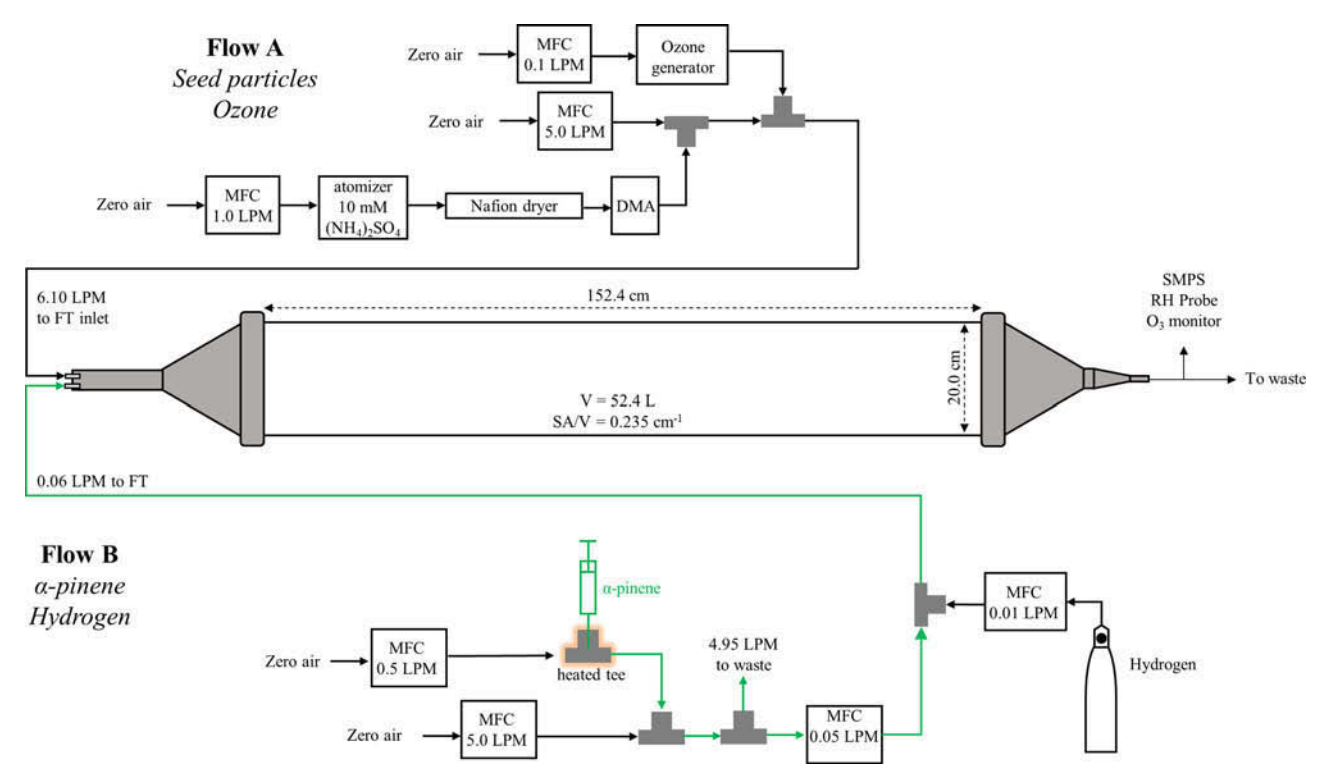


Figure 1. Experimental setup and flow tube reactor. Flow A contains seed particles and ozone while Flow B contains  $\alpha$ -pinene vapor and hydrogen gas.

2c and 3 of Ehn et al. (2014) and Figure 1d of Tröstl et al. (2016), suggesting that there may be a systematic error associated with gas phase measurements.

In the work presented here, we measure changes in the diameter of seed particles in the 40-80 nm size range when they are exposed to the products of α-pinene ozonolysis in a flow tube reactor. Measured particle growth is combined with a kinetic model to confirm a condensational growth mechanism and determine the molar yield of condensable organic molecules for particles in this size range. For readability and consistency with the literature, we refer to the yield measured here as a "HOM" yield. However, the yield we obtain from particle size measurements is not exactly the same parameter as that obtained from gas phase measurements. The relationship between the two will be discussed.

# 2. Experimental section

# 2.1. Flow tube reactor

The flow tube reactor and experimental setup used in this work are shown in Figure 1. The reactor consists of a quartz tube 150 cm long and 20 cm i.d. with stainless steel funnels extending from both ends. These funnels are 18 cm long and taper down to a final i.d. of 5 cm. The total volume of the reactor assembly is 52 L.

The optimum air flow rate through the reactor was determined experimentally by injecting 30 s plugs of 60 nm dia. ammonium sulfate particles through the flow tube and measuring the particle number concentration at the exit as a function of time with a condensational particle counter (3788 CPC, TSI Inc., Shoreview, Minnesota). The goal was to experimentally determine the air flow conditions that produced the smallest distribution of particle residence times in the flow reactor. From these experiments, it was determined that a 6 L/min major air flow rate (Flow A in Figure 1) produced a narrow range of residence times while at the same time minimizing the impact of air recirculation in the tube. Figure 2 shows the residence time distribution of particles using these flows. The average distribution was determined from five individual plug injections and the shaded region of the figure shows one standard deviation. The peak of the distribution was  $232 \pm 15$  s, and the full width at half maximum was 81 s. A small recirculation peak was observed at slightly more than twice the average residence time, but recirculation consistently represented less than 10% of the total distribution.

# 2.2. CFD simulations

The flow tube reactor used in this work was recreated in COMSOL Multiphysics 5.3a (Stockholm, Sweden,

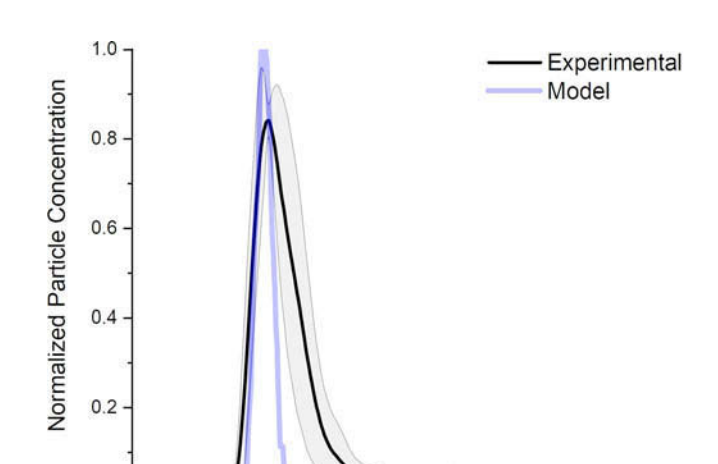


**Figure 2.** Residence time distribution of particles exiting flow tube. Dark line shows average distribution of five trials. The gray shaded region represents one standard deviation. The blue line represents the modeled residence time using the particle tracing module in COMSOL.

Time After Injection (min)

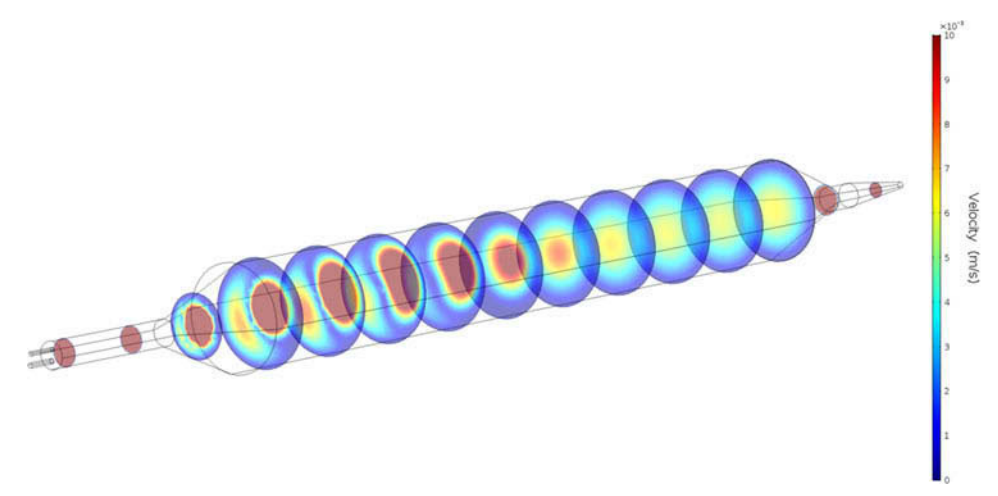


Figure 3. Calculated velocity through the flow tube shown as vertical slices along the length of the reactor.

http://www.comsol.com) to perform computational fluid dynamics (CFD) calculations to characterize the flow throughout the reactor and compare with experimental measurements. The flow tube geometry was recreated in COMSOL as a 3-D model, and COMSOL's finite element method was used to solve for flows throughout. The geometry was meshed using a normal sized free tetrahedral mesh consisting of  $2 \times 10^5$  elements with an average quality of 0.66. The element quality is a measure of cell distortion with a value of 1 indicating perfect element shape. The model was tested using finer mesh densities to ensure reproducible results and no mesh dependence was observed. Once meshed, a stationary laminar flow model was solved using the inlet flows used in the growth experiments; 6.1 L/min in Flow A and 0.06 L/ min in Flow B and the flow of the outlet was assumed

0.0

to be at atmospheric pressure. The evolution of the flow profile is shown in Figure 3 by velocity slices down the length of the tube. A laminar flow profile develops quickly in the initial mixing tube before expansion. Once the flow reaches the reactor and begins to expand, a recirculation zone appears in the area the main flow has not occupied. This recirculation persists to about half way into the tube, where a laminar profile is reestablished throughout the entire width of the tube and maintained the rest of the way including the reduction in diameter to the outlet. Similar recirculation regions have been observed in other CFD studies of flow tube reactors (Huang et al. 2017).

The particle tracing module within COMSOL was coupled to the CFD model to calculate the distribution of particle residence times in the flow tube. For

these calculations, 300 particles with an 80 nm diameter were released over a 30 s period from the Flow A inlet as a density function from the center, and the times at which they exited the assembly were traced. The calculated and measured residence times show excellent agreement as shown in Figure 2. Since no particles in the simulation entered the recirculation region, the small recirculation peak in the experimental data was not replicated in the simulation. Gasphase species, however, distribute evenly across the different regions of the flow tube, and if the system is given enough time to reach steady state, the gas phase mixing ratio becomes independent of location in the flow tube. As discussed later, the calculated equilibration time matches the measurement.

# 2.3. Particle growth experiments

For the experiments described here, the major flow (Flow A in Figure 1) contained seed particles and ozone, while the minor flow (Flow B in Figure 1) contained α-pinene and hydrogen gas (99.999% Keen Gas, Newark, DE). Ammonium sulfate seed particles were generated by atomizing (TOPAS ATM226, Dresden, Germany) a solution of ammonium sulfate (99.9995%, Sigma-Aldrich Co., St. Louis, MO). The resulting polydisperse aerosol was sent through a Nafion dryer (MD-700, Perma Pure, Lakewood, NJ) to decrease the relative humidity (RH) of the surrounding air to 10%, which is substantially below the efflorescence RH of ammonium sulfate  $(35 \pm 2\%)$  at 298 K) (Ciobanu et al. 2010). The dry particles were then size-selected with a model 3080 classifier and model 3085 differential mobility analyzer (DMA) both from TSI Inc. The flow of monodisperse particles was mixed with ozone and sent into the flow tube. Ozone was generated from an ozone monitor (model 42C, Thermo Fischer Scientific Inc., Waltham, MA), and the mixing ratio was adjusted by changing the lamp intensity. All flows were maintained by mass flow (MFC, Dakota controllers Instruments Orangeburg, NY). The flow tube temperature for these experiments was 297 K.

Liquid α-pinene (Sigma–Aldrich Co.) was injected at a rate of 0.05 µL/min into a gently heated air flow of 50 mL/min using a 100 μL syringe (Hamilton Company, Reno, NV) and a syringe pump (New Era Pump Systems Inc., Farmingdale, NY). This air flow was mixed with a larger flow of 5 L/min to dilute the vapor, and then 50 mL/min of the diluted air flow was sent into the reactor. For the experiments described here, the mixing ratio of  $\alpha$ -pinene in the flow tube was 11 ppbv. A small flow of 10 mL/min of hydrogen gas was mixed with the  $\alpha$ -pinene flow before entering the tube. The hydrogen was added to act as an OH scavenger (Sarnela et al. 2018) and had a final concentration of 0.1% by volume. The addition of an OH scavenger is necessary as the hydroxyl radical is produced by  $\alpha$ -pinene ozonolysis with a reported yield of 85% (Calvert 2008) and could complicate the interpretation of results by reacting with additional α-pinene molecules. While the reported HOM yield from OH oxidation is almost an order of magnitude lower than that of ozone oxidation (Jokinen et al. 2015), it is important to scavenge the OH to ensure that the measured HOM yield is specifically for the ozonolysis reaction.

Aerosol exiting the flow tube was monitored with a scanning mobility particle sizer (SMPS; TSI Inc.), an ozone monitor (Model 49i, Thermo Fisher Scientific Inc.) and an RH probe (Traceable, Thermo Fisher Scientific Inc.). The SMPS used here consisted of a 3081 DMA and 3788 CPC to scan the particle distribution between 10 and 400 nm mobility diameter every 2 min.

The experiments described here were conducted by first introducing seed particles along with ozone at its lowest mixing ratio of approximately 30 ppbv. The addition of ozone did not cause any change in the particle size distribution. Once the system stabilized, α-pinene was introduced, giving a mixing ratio of 11 ppbv in the flow tube. The system was allowed to stabilize until consistent (<10% variation) ozone mixing ratio, particle size distribution and number concentration were obtained for at least 15 min. After stabilization, the lamp intensity and corresponding ozone mixing ratio were systematically incremented. In total, five ozone mixing ratios were investigated, which spanned the range 30-250 ppbv.

Molecular composition measurements by high-resolution electrospray ionization mass spectrometry (ESI-MS) were performed using a Thermo Q-Exactive Orbitrap mass spectrometer to characterize the organic material condensing onto the particles. For these measurements particles were collected onto a quartz microfiber filter (GF/D, Whatman, Maidstone, UK) at the exit of the flow tube using the highest ozone mixing ratio (250 ppbv) and middle seed particle diameter (60 nm). The organic material was then extracted using acetonitrile (Optima grade, Fisher Scientific, Hampton, NH) and concentrated under vacuum to a final concentration of approximately 0.1 μg/μL. This extract was then analyzed using direct infusion on the Orbitrap operated in negative mode.

Data processing and formula assignment of the resulting mass spectra was then performed as described in Tu, Hall, and Johnston (2016).

# 2.4. Modeling particle growth

The amount of seed particle growth obtained for each ozone increment was evaluated with respect to the formation of HOMs produced by  $\alpha$ -pinene ozonolysis. Modeling the formation of HOMs was done recursively by updating reactant and product concentrations each second for the duration of the flow tube residence time. Once the gas phase concentration is calculated, it can then be used to predict the diameter change of a particle, assuming that condensation is a collision-limited process, using Equation (1) adapted from Apsokardu and Johnston (2018):

$$\frac{\partial d}{\partial t} = \frac{c}{2} \gamma [\text{HOM}]_t \beta_{\text{d}} V_{\text{HOM}}, \tag{1}$$

where c is the mean thermal velocity,  $\gamma$  is the uptake coefficient (assumed to be 1 in this work),  $[HOM]_t$  is the time-dependent gas-phase HOM mixing ratio,  $\beta_d$  is the mass flux correction factor and  $V_{HOM}$  is the molecular volume. For these calculations, HOMs were assumed to have an average molecular weight of  $200 \, \text{g/mol}$  and a density of  $1.2 \, \text{g/cm}^3$ . The predicted diameter change can then be fit to the experimental data by adjusting the HOM yield and thus the HOM mixing ratio.

Multiple processes occurring within the tube are accounted for in the model. First is the oxidation of  $\alpha$ -pinene by ozone, based on the respective mixing ratios and a second order rate constant ( $k_{\rm II}$ ) of  $8.4\times10^{-17}\,{\rm cm}^3$  molec<sup>-1</sup> s<sup>-1</sup> (Khamaganov and Hites 2001). Second is the formation of HOMs from the ozonolysis reaction, which will be discussed in detail in the results and discussion section. Third is wall loss of HOMs, modeled as a diffusion limited process based on Hanson and Eisele (2000) and accounting for entry effects discussed in Knopf, Pöschl, and Shiraiwa (2015):

$$k_{\rm WL} = N_{\rm Shw}^{\rm eff} \frac{D}{r^2},\tag{2}$$

where  $k_{\rm WL}$  is the wall loss rate constant,  $N_{\rm Shw}^{\rm eff}$  is the effective Sherwood number, r is the radius of the flow tube, D is the gas phase diffusion coefficient, and it is assumed that HOMs are nonvolatile enough that the sticking probability is 1. The Sherwood number was varied to account for entry effects in the beginning of the flow tube. However, this did not have a significant effect on HOM mixing ratio in the flow tube since

only a small amount of HOMs are produced in this region. Modeling wall loss in this way gives an average  $k_{\rm WL} = 2.0 \times 10^{-3}~{\rm s}^{-1}$  assuming a constant flow tube radius of 10 cm.

In addition to the constant radius calculation above, wall loss was also approximated by varying the effective diameter in the various stages of the flow tube assembly. For this calculation, particle residence time in the initial mixing tube was 3 s, and the radius for wall loss during this time period was taken as the 2.375 cm radius of the tube. During expansion in the funnel and first part of the flow tube, the effective radius increased from 2.375 to 10 cm at the point where laminar flow was fully established across the width of the flow tube. The particle residence time in this expanding region was 60 s, and it was assumed that the effective diameter for wall loss increased linearly with time in this region. The radius was then held constant at 10 cm for the remaining portion of the flow tube, which covered a period of 124 s. Finally, the radius was assumed to decrease linearly from 10 cm back to 2.375 cm over the final 38 s spent in the outlet funnel. Modeling wall loss in this way gave a time averaged  $k_{\rm WL} = 6.4 \times 10^{-3} \ \rm s^{-1}$ . As discussed later, the difference between these two methods of calculating wall loss did not give an appreciable difference in the calculated molar yield of HOMs.

The final process accounted for in the model was loss of HOM to the condensation sink. The condensation sink was calculated for each size distribution according to Equation (3) adapted from Dal Maso et al. (2002).

$$k_{\rm CS} = 2\pi D \sum \beta_{\rm di} d_{\rm pi} N_i, \tag{3}$$

where  $k_{CS}$  is the first order rate constant for loss to the condensation sink,  $d_{pi}$  is the particle diameter and  $N_i$  is the number concentration at the diameter. However, the value of the condensation sink is not constant throughout the flow tube as the size distribution begins as the seed distribution and evolves over the residence time of the tube into what is measured at the end. For this reason, we begin with the condensation sink as the value calculated from the seed distribution and increase it as a function of  $t^2$  as discussed by Ezhova et al. (2018). Because the condensation sink increases at most by a factor of two in these experiments, the assumed time dependence does not have a significant impact on the calculations. However, the condensation sink is very different for the three size-selected aerosols studied in this work, so it is imperative to consider its effect on particle growth.



Taking the discussed processes into account, HOM production can be summarized by Equation (4):

$$[HOM]_{t+\Delta t} = [HOM]_t + k_{II} [\alpha P]_t [O_3]_t y \Delta t$$
$$-k_{WL} [HOM]_t \Delta t - k_{CS} [HOM]_t \Delta t, \quad (4)$$

where  $[HOM]_t$ ,  $[\alpha P]_t$  and  $[O_3]_t$  are the respective mixing ratios at time t,  $\Delta t$  is the time increment,  $k_{\rm II}$  is the second order rate constant, and y is the molar yield of HOM for  $\alpha$ -pinene ozonolysis.

Figure 4 gives examples of this calculation for the α-pinene and ozone mixing ratios used in the experiment with 40 nm dia. seed particles. Figure 4a shows the HOM mixing ratio and Figure 4b shows the HOM exposure (pptv-s), both as a function of time in the flow tube. Because HOM mixing ratio builds up slowly at the beginning of the flow tube, the incompletely developed laminar flow profile (Figure 3) exerts a relatively small effect on HOM mixing ratio and exposure at the outlet. These calculations assume a HOM yield of 12.5% and use the constant tube radius method of determining wall loss. HOM exposure is obtained by integrating the HOM mixing ratios as shown in Equation (5):

$$E_t = \int_{t=0}^t [\text{HOM}]_t dt, \tag{5}$$

where  $E_t$  is total exposure at time t in the flow tube. At the flow tube exit, the HOM mixing ratio and exposure increase approximately linearly with ozone mixing ratio under the conditions used the experiment.

In the work that follows, the calculated particle diameter at the flow tube exit is determined by integrating Equation (1) over time using the time-dependent HOM mixing ratio determined from Equation (4).

# 3. Results and discussion

# 3.1. Particle growth measurements

Seed particle growth by  $\alpha$ -pinene ozonolysis was studied as a function of particle diameter and ozonolysis reaction rate. The reaction rate was systematically varied through successive increments of the ozone mixing ratio. The seed particles were composed of ammonium sulfate at low RH (10%), rendering them nominally unreactive with respect to particle-phase chemical processes.

One such experiment is shown in Figure 5 starting with 40 nm dia. seed particles. At the start of the experiment, seed particles and ozone were sent through the reactor and a stable flow was achieved. At

the time point indicated by the vertical dashed green line, α-pinene vapor was introduced, which caused the seed particles to grow as indicated by increases in the median diameter (third panel) and volume (fourth panel) of the aerosol. After the size distribution stabilized, the ozone mixing ratio was incremented up to the next value. The median diameter and volume increased again, and after the new size distribution stabilized, this process was repeated. In all, four ozone increments were performed, and their time points are shown as vertical dashed gray lines in Figure 5. The time between ozone increments was approximately 1 h as it took the reactor close to 30 min to reach steadystate and then particle size distributions were averaged over the remaining time period. The experimentally observed equilibration time period for gas phase reactants matched the CFD calculated time period, providing an additional consistency check between measured and calculated flow properties.

An interesting feature of Figure 5 is the much smaller fluctuation of the median diameter than the aerosol volume. We attribute the variation in the aerosol volume measurement mainly to fluctuation of the aerosol output by the atomizer. Superimposed on this fluctuation may be an additional contribution from the measurement uncertainty of the SMPS. Since neither of these variations affects particle residence time in the reactor, the median diameter of the aerosol is a more precise indicator of particle growth. While equations exist to fit the entire size distribution and normalize variations in residence times such as those outlined in Kuwata and Martin (2012), they could not be directly used in this work because of the nonuniform HOM mixing ratio throughout the tube. Instead, median diameter is used as an indicator for particle growth, because the precision and reproducibility of the measurement are better.

Particle growth is also indicated by changes in the average size distribution for each ozone increment. Particle size distributions for the experiment in Figure 5 are shown in Figure 6a. The time periods over which size distributions were averaged are shown as horizontal bars just above the ozone plot in Figure 5. With each ozone increment, the distribution shifts to a larger particle size and broadens. This broadening and its characteristic tail to the high diameter side of the distribution are attributed to the shape of the residence time distribution in Figure 2. In addition, there is a second peak observed, caused by doubly charged seed particles that passed through the DMA used for size selection and subsequently lost a charge prior to analysis by SMPS at the flow tube exit.

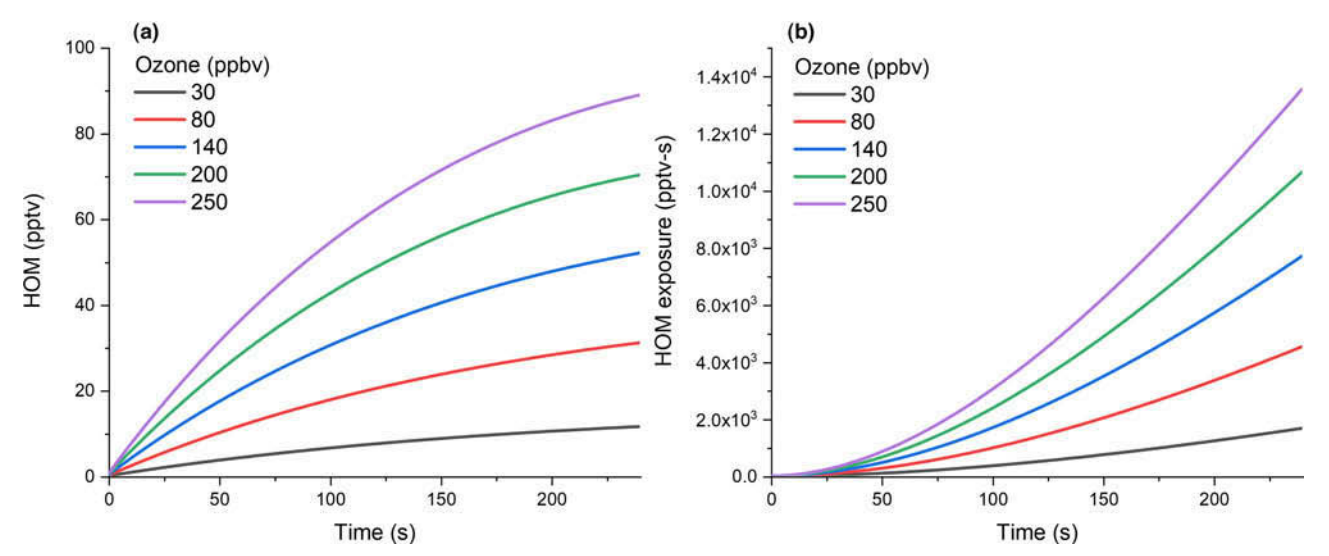


Figure 4. Calculated mixing ratio (a) and exposure (b) of HOMs for each ozone concentration over the residence time of the flow tube. These plots used a molar yield of 12.5% for  $\alpha$ -pinene ozonolysis with wall loss modeled as a constant diameter and condensation sink (seed particles of 40 nm) for the experiment shown in Figure 5.

The experiment in Figure 5 was repeated for 60 and 80 nm dia. seed particles. Plots for these experiments are shown in Figures S1 and S2, respectively, and the size distributions are shown in Figure 6b and c. For each seed particle size, the distribution shifts to a larger particle diameter and broadens as the ozone mixing ratio increases. The linear scale for particle diameter is shifted among the plots in Figure 6 to align the seed particle size distributions vertically, which illustrates a key observation in these experiments. The diameter growth of larger diameter seed particles is less than that observed for smaller diameter seed particles. This phenomenon and other details of particle growth are discussed below.

# 3.2. Mechanism of particle growth

The experimental results in Figures 5 and 6 are summarized in Figure 7, where the change in median diameter (difference between median diameter with and without  $\alpha$ -pinene ozonolysis) is plotted vs. ozone mixing ratio. In all, data from six separate experiments are shown, two repeat experiments for each of the three seed particle sizes. The replicate trials at each initial seed diameter show good agreement, and the diameter growth for each seed size is linear with increasing ozone mixing ratio.

Apsokardu and Johnston (2018) have discussed the particle size dependence of growth rates for different growth mechanisms. The growth rate is, to a first approximation, independent of particle diameter for growth processes limited by the condensation rate of gas phase precursors. Examples include condensation

of nonvolatile compounds whose evaporation rates are negligible, and uptake of semivolatile compounds that react so quickly in the particle phase to give a nonvolatile product that their uptake is limited by the condensation rate. In contrast, uptake of semivolatile compounds by reaction in the particle phase at a rate slower than the collision-limited condensation rate would exhibit an increasing growth rate with increasing particle size. For the growth experiments performed here, dry ammonium sulfate seed particles are expected to be inert with respect to particle-phase chemistry. Therefore, growth is expected to be independent of seed particle diameter assuming that the condensation sink remains constant. However, the condensation sink is very different for the 40, 60, and 80 nm seed particle diameter experiments. As discussed below, it is condensation sink associated with the different seed particles, rather than particle diameter itself, that leads to the differences among the plots in Figure 7.

The modeling approach described in Section 2.4 was used to calculate expected diameter increases for comparison with the experimental data in Figure 7. The only parameter in the calculation that is different for the three particle sizes is the condensation sink for the aerosol in each experiment. All other parameters are fixed, except for the molar yield of HOM for the ozonolysis reaction (y in Equation (4)), which is adjusted to fit the calculated data to the experimental data. The solid lines in Figure 7 show the best-fit calculated diameter changes assuming a HOM molar yield of 12.5% and wall loss based on a constant 10 cm radius. The method used to calculate wall loss

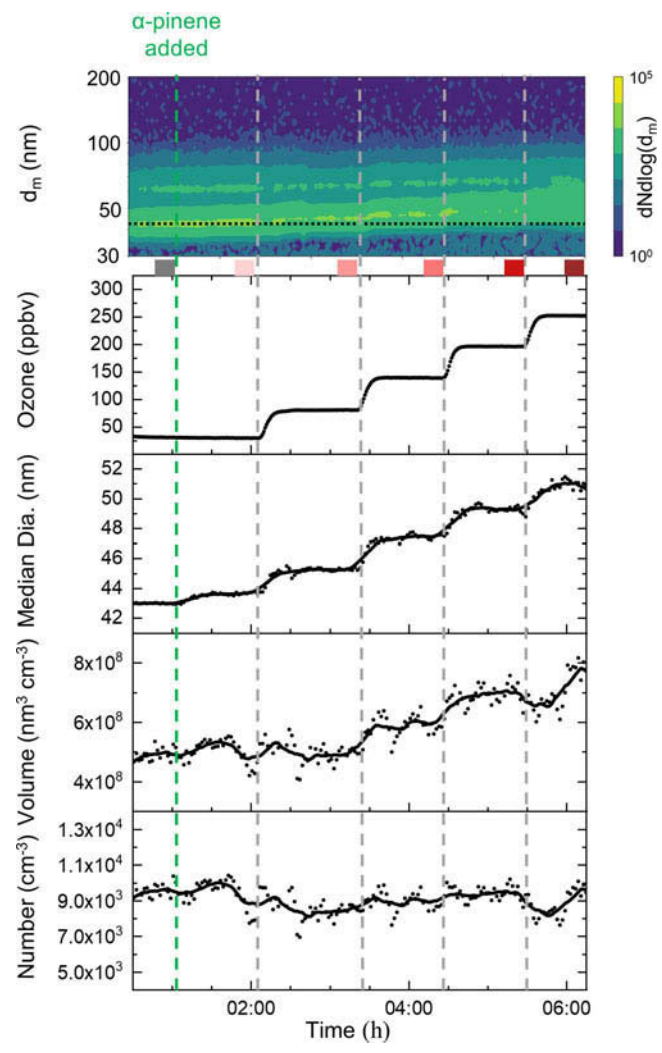


**Figure 5.** Growth experiment of 40 nm ammonium sulfate seed particles. At the top is a contour plot of aerosol size distribution measured by SMPS, followed by ozone mixing ratio, median particle diameter, volume and particle number concentration exiting the flow tube. The green vertical line indicates when  $\alpha$ -pinene vapor injection began. Gray vertical lines indicate when increments of the ozone mixing ratio were made. Dots represent raw data and the black lines are ten-point moving averages. Bars below the contour plot indicate the time where data were averaged for further analysis.

only slightly affects the HOM yield derived from the modeling. If, instead, wall loss is calculated using the varying radius approach, the molar yield needed to fit the data is 13.5%. For either method of calculating wall loss, changing the HOM molar yield by as little as  $\pm 0.5\%$  caused the solid lines to deviate significantly from the experimental data. Taking all of these observations into account, we report the molar yield of HOM to be  $13 \pm 1\%$ .

The electrospray ionization mass spectrum of particles that were collected from the 250 ppbv ozone experiment with 60 nm seed particles is shown in Figure S3. The mass spectrum is dominated by  $C_xH_yO_z$  species having  $x \le 10$ , i.e., monomers. Molecular formulas assigned from Figure S3 do not closely match formulas assigned from chemical

ionization measurements of HOMs. This difference has been noted in previous studies and is attributed to decomposition of gas-phase HOMs once they enter the particle phase (Zhang et al. 2017; Krapf et al. 2016; Tu, Hall, and Johnston 2016; Mutzel et al. 2015). While a correspondence of Figure S3 with gasphase HOM measurements is not expected, Figure S3 does provide insight for the discussion below. First, dimer signal intensities are very low. Since most dimer species are thought to be formed directly in the particle phase as discussed by Shiraiwa et al. (2014), it is unlikely that oligomerization in the particle phase contributed significantly to particle growth in these experiments. Second, there is no evidence of organosulfate formation, ruling out this pathway as a significant contributor to particle growth.

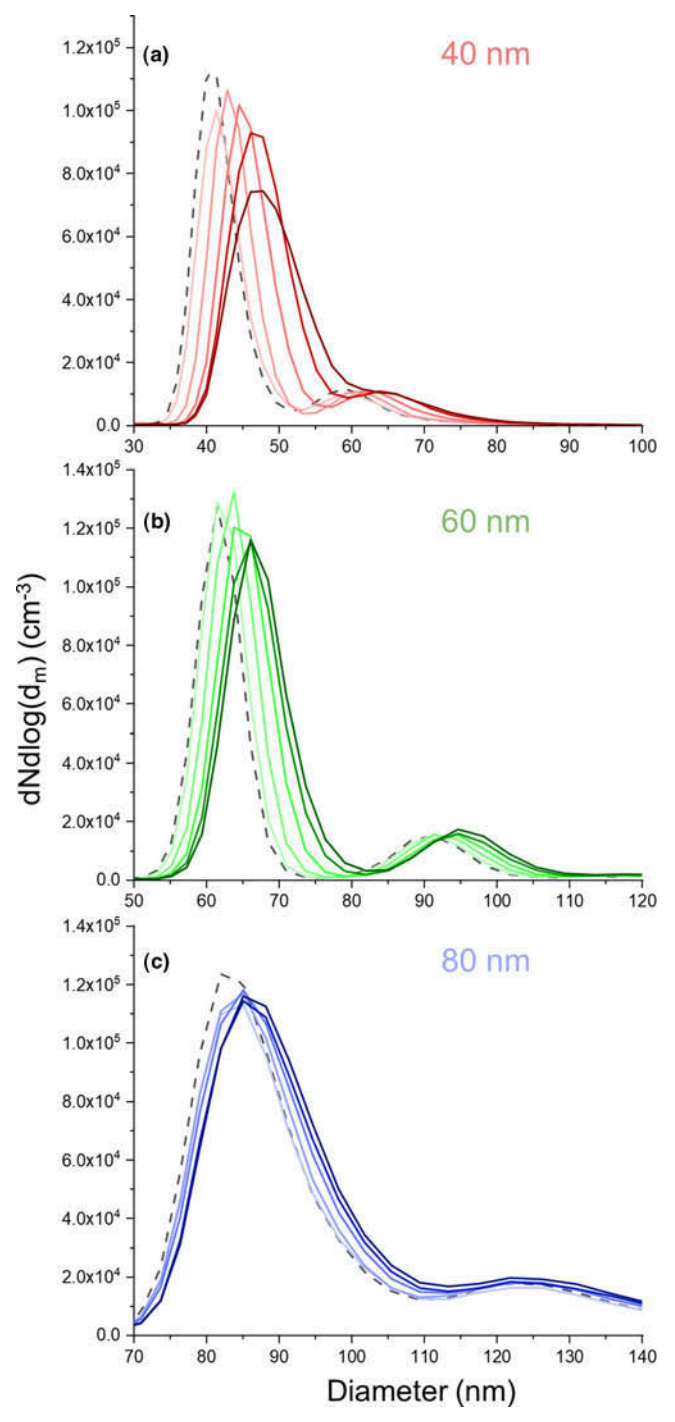


**Figure 6.** Average size distribution for each ozone mixing ratio in experiments with 40, 60, and 80 nm dia. seed particles. Approximate ozone mixing ratios are 30, 80, 140, 200, and 250 ppbv.

# 3.3. Comparison of yields based on gas vs. Particle phase measurements

Table 1 compares the molar yield of condensable organic molecules obtained from particle growth measurements in this work to molar yields of HOMs from previous gas-phase measurements with  $\mathrm{NO_3}^-$  chemical ionization. Our reported yield (13%) is somewhat higher than the yields determined from

gas-phase measurements (3–7%). Three factors that may contribute to this difference.

First is the character of gas-phase measurements. HOM yields are based on a specific set of ions detected with  $\mathrm{NO_3}^-$  chemical ionization, the assumptions being that all relevant species are detected by this method and the ionization yield (fraction of molecules entering the mass spectrometer source region

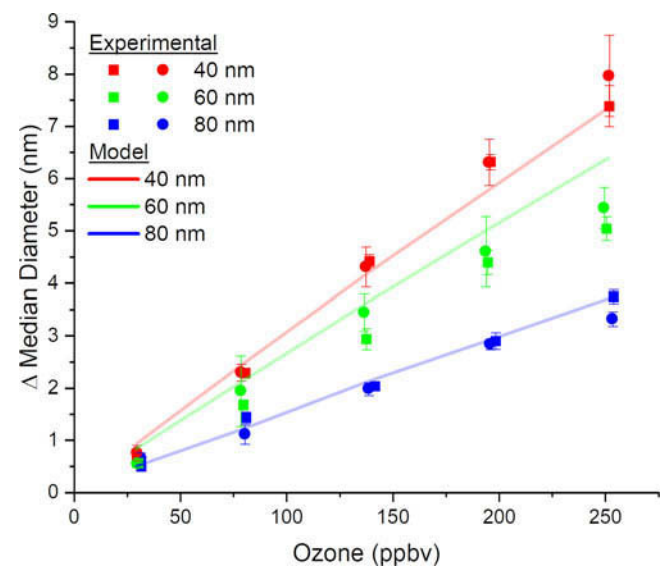


Figure 7. Seed particle growth (increase in median diameter) vs. ozone mixing ratio. Squares and circles represent duplicate experiments with error bars representing one standard deviation. The lines represent predicted particle growth using modeling as described in Section 2.4 with a molar yield of 12.5% for formation of HOMs from  $\alpha$ -pinene ozonolysis.

that are ionized) is fixed and known. However, if some species are not detected, then the actual HOM yield will be greater than the measured yield. We note that measured particle growth tends to be underestimated by chemical ionization measurements (Ehn et al. 2014; Tröstl et al. 2016), which suggests that some relevant species may not be detected.

Second is the character of particle-phase measurements. HOMs are thought to be highly reactive molecules that can decompose quickly in the particle phase (Krapf et al. 2016). If decomposition leads to formation of a more volatile product, then evaporation of the product will decrease the particle size and give a smaller apparent growth rate than predicted by HOM condensation alone. In the current experiment, the short residence time of particles in the flow tube minimizes this effect. Alternatively, it is possible that heterogeneous chemical reactions, i.e., reactions that occur within the condensed phase or at the interface between phases, could assist particle growth if they transform relatively volatile molecules that strike the particle surface into nonvolatile products that stay in the particle phase. In this case, particle growth would be greater than that predicted by condensation of HOMs alone since a wider range of molecular species contribute to growth. The molecular composition measurements in this work rule out particle phase chemistry associated with oligomer and organosulfate formation. However, it is possible that other types of reactions may occur, particularly those occurring at an interface. If we assume a core-shell morphology

for particles exiting the flow tube, i.e., a liquid secondary organic layer surrounding a solid inorganic core, then the thickness of the organic layer of particles exiting the flow tube is at most a few nanometers and the surface-to-volume ratio is high. Therefore, surface chemistry could have a rather large impact on particle growth.

Third is the impact of experimental conditions. An important difference between the gas-phase studies in Table 1 and ours is RH. If formation of the stabilized Crieegie Intermediate (sCI) is a step in the formation of HOMs, then it is possible for RH to have a direct effect on measured HOM yield as water has been shown to react with sCI (Newland et al. 2018; Berndt et al. 2014) reducing the HOMs produced and lowering the yield with increasing RH. Therefore, the higher yield reported in our work could be due in part to the lower RH. Another important difference is particle size. Most of the gas-phase experiments in Table 1 were focused on growth of particles on the order of a few nanometers. In this size range, the Kelvin effect exerts a huge impact on molecular volatility, and the range of molecules that can lead to particle growth is much smaller than for Aitken mode particles where the Kelvin effect is insignificant. We note that the molar yields determined by Jokinen et al. (2015) and Kirkby et al. (2016) excluded HOMs thought to be unimportant for growth of small nanoparticles, and their yields are much smaller than ours. The Ehn et al. (2014) study did include a measurement of Aitken mode particle growth, and their yield

is closest to ours. Future studies will focus on higher RH and different seed particle compositions to elucidate their roles in particle growth.

# 4. Conclusions

We have investigated the growth of size-selected ammonium sulfate seed particles in the 40-80 nm range by α-pinene ozonolysis under dry conditions. The increase in seed particle diameter was consistent with a collision-limited condensational growth mechanism, and the magnitude of the increase allowed the molar yield of condensable organic molecules from α-pinene ozonolysis to be determined. The reported HOM yield,  $13 \pm 1\%$ , is somewhat higher than reported yields of HOMs measured in the gas phase with NO<sub>3</sub><sup>-</sup> chemical ionization mass spectrometry. Potential reasons for this difference were discussed including factors inherent to gas phase measurements, particle phase measurements, and the experimental conditions of the various studies.

# **Funding**

This research was supported by the U.S. National Science Foundation under grant numbers AGS-1649694 (SHL) and AGS-1649719 (MVJ).

## **ORCID**

Justin M. Krasnomowitz http://orcid.org/0000-0002-

Michael J. Apsokardu http://orcid.org/0000-0001-9835-7259

Christopher M. Stangl (b) http://orcid.org/0000-0003-

Lee Tiszenkel (D) http://orcid.org/0000-0002-2117-8292 Qi Ouyang http://orcid.org/0000-0002-4211-102X Shanhu Lee http://orcid.org/0000-0001-7702-6960 Murray V. Johnston http://orcid.org/0000-0001-9529-8660

# References

- Apsokardu, M. J., and M. V. Johnston. 2018. Nanoparticle growth by particle-phase chemistry. Atmos. Chem. Phys. 18 (3):1895-1907. doi:10.5194/acp-18-1895-2018.
- Berndt, T., T. Jokinen, M. Sipilä, R. L. Mauldin, H. Herrmann, F. Stratmann, H. Junninen, and M. Kulmala. 2014. H<sub>2</sub>SO<sub>4</sub> formation from the gas-phase reaction of stabilized Criegee intermediates with SO2: Influence of water vapour content and temperature. Atmos. Environ. 89:603-612. doi:10.1016/j.atmosenv.2014.02.062.

- Calvert, J. G. 2008. The mechanisms of atmospheric oxidation of the alkenes. Oxford, New York: Oxford University
- Ciobanu, V. G., C. Marcolli, U. K. Krieger, A. Zuend, and T. Peter. 2010. Evidence for surface nucleation: Efflorescence of ammonium sulfate and coated ammonium sulfate aerosol particles. J. Phys. Chem. A 114 (35): 9486-9495. doi:10.1021/jp103541w.
- Crounse, J. D., L. B. Nielsen, S. Jørgensen, H. G. Kjaergaard, and P. O. Wennberg. 2013. Autoxidation of organic compounds in the atmosphere. J. Phys. Chem. Lett. 4 (20):3513-3520. doi:10.1021/jz4019207.
- Dal Maso, M., M. Kulmala, K. E. J. Lehtinen, J. M. Mäkelä, P. Aalto, and C. D. O'Dowd. 2002. Condensation and coagulation sinks and formation of nucleation mode particles in coastal and boreal forest boundary layers. J. Geophys. Res.: Atmos. 107 (D19):PAR-2. doi:10.1029/ 2001JD001053.
- Donahue, N. M., S. A. Epstein, S. N. Pandis, and A. L. Robinson. 2011. A two-dimensional volatility basis set: 1. Organic-aerosol mixing thermodynamics. Atmos. Chem. Phys. 11 (7):3303-3318. doi:10.5194/acp-11-3303-2011.
- Donahue, N. M., J. H. Kroll, S. N. Pandis, and A. L. Robinson. 2012. A two-dimensional volatility basis set— Part 2: Diagnostics of organic-aerosol evolution. Atmos. Chem. Phys. 12 (2):615-634. doi:10.5194/acp-12-615-2012.
- Dusek, U., G. P. Frank, L. Hildebrandt, J. Curtius, J. Schneider, S. Walter, D. Chand, F. Drewnick, S. Hings, D. Jung, et al. 2006. Size matters more than chemistry aerosol particles. Science 312 (5778):1375-1378. doi: 10.1126/science.1125261.
- Ehn, M., E. Kleist, H. Junninen, T. Petäjä, G. Lönn, S. Schobesberger, M. Dal Maso, A. Trimborn, M. Kulmala, D. R. Worsnop, et al. 2012. Gas phase formation of extremely oxidized pinene reaction products in chamber and ambient air. Atmos. Chem. Phys. 12 (11):5113-5127. doi:10.5194/acp-12-5113-2012.
- Ehn, M., J. A. Thornton, E. Kleist, M. Sipilä, H. Junninen, I. Pullinen, M. Springer, F. Rubach, R. Tillmann, B. Lee, et al. 2014. A large source of low-volatility secondary organic aerosol. Nature 506 (7489):476-479. doi:10.1038/ nature13032.
- Ezhova, E., V. M. Kerminen, K. E. J. Lehtinen, and M. Kulmala. 2018. A simple model for the time evolution of the condensation sink in the atmosphere for intermediate Knudsen numbers. Atmos. Chem. Phys. 18 (4):2431-2442. doi:10.5194/acp-18-2431-2018.
- Hallquist, M., J. C. Wenger, U. Baltensperger, Y. Rudich, D. Simpson, M. Claeys, J. Dommen, N. M. Donahue, C. George, A. H. Goldstein, et al. 2009. The formation, properties and impact of secondary organic aerosol: Current and emerging issues. Atmos. Chem. Phys. 9 (14): 5155-5236. doi:10.5194/acp-9-5155-2009.
- Hanson, D. R., and F. Eisele. 2000. Diffusion of H<sub>2</sub>SO<sub>4</sub> in humidified nitrogen: Hydrated H<sub>2</sub>SO<sub>4</sub>. J. Phys. Chem. A 104 (8):1715-1719. doi:10.1021/jp993622j.
- Huang, Y., M. M. Coggon, R. Zhao, H. Lignell, M. U. Bauer, R. C. Flagan, and J. H. Seinfeld. 2017. The caltech photooxidation flow tube reactor: Design, fluid dynamics and characterization. Atmos. Meas. Tech. 10 (3):839-867. doi:10.5194/amt-10-839-2017.



- Jimenez, J. L., M. R. Canagaratna, N. M. Donahue, A. S. H. Prevot, Q. Zhang, J. H. Kroll, P. F. DeCarlo, J. D. Allan, H. Coe, N. L. Ng, et al. 2009. Evolution of organic aerosols in the atmosphere. Science 326 (5959):1525-1529. doi:10.1126/science.1180353.
- Jokinen, T., T. Berndt, R. Makkonen, V.-M. Kerminen, H. Junninen, P. Paasonen, F. Stratmann, H. Herrmann, A. B. Guenther, D. R. Worsnop, et al. 2015. Production of extremely low volatile organic compounds from biogenic emissions: Measured vields and atmospheric implications. Proc. Natl. Acad. Sci. USA 112 (23):7123-7128. doi:10.1073/pnas.1423977112.
- Khamaganov, V. G., and R. A. Hites. 2001. Rate constants for the gas-phase reactions of ozone with isoprene,  $\alpha$ - and  $\beta$ -pinene, and limonene as a function of temperature. J. Phys. Chem. A 105 (5):815-822. doi:10.1021/jp002730z.
- Kirkby, J., J. Duplissy, K. Sengupta, C. Frege, H. Gordon, C. Williamson, M. Heinritzi, M. Simon, C. Yan, J. Almeida, et al. 2016. Ion-induced nucleation of pure biogenic particles. Nature 533 (7604):521-526. doi:10.1038/nature17953.
- Knopf, D. A., U. Pöschl, and M. Shiraiwa. 2015. Radial diffusion and penetration of gas molecules and aerosol particles through laminar flow reactors, denuders, and sampling tubes. Anal. Chem. 87 (7):3746-3754. doi:10.1021/ac5042395.
- Komppula, M., H. Lihavainen, J. Hatakka, J. Paatero, P. Aalto, M. Kulmala, and Y. Viisanen. 2003. Observations of new particle formation and size distributions at two different heights and surroundings in subarctic area in Northern Finland. J. Geophys. Res.: Atmos. 108 (D9):4295. doi:10.1029/2002JD002939.
- Komppula, M., H. Lihavainen, V. M. Kerminen, M. Kulmala, and Y. Viisanen. 2005. Measurements of cloud droplet activation of aerosol particles at a clean subarctic background site. J. Geophys. Res. D: Atmos. 110 (6):1-10. doi:10.1029/2004JD005200.
- Krapf, M., I. El Haddad, E. A. Bruns, U. Molteni, K. R. Daellenbach, A. S. H. Prévôt, U. Baltensperger, and J. Dommen. 2016. Labile peroxides in secondary organic aerosol. Chem 1 (4):603-616.doi:10.1016/ j.chempr.2016.09.007.
- Kulmala, M., J. Kontkanen, H. Junninen, K. Lehtipalo, H. E. Manninen, T. Nieminen, T. Petaja, M. Sipila, S. Schobesberger, P. Rantala, et al. 2013. Direct observations of atmospheric aerosol nucleation. Science 339 (6122): 943-947. doi:10.1126/science.1227385.
- Kuwata, M., and S. T. Martin. 2012. Particle size distributions following condensational growth in continuous flow aerosol reactors as derived from residence time distributions: Theoretical development and application to secondary organic aerosol. Aerosol Sci. Technol. 46 (8): 937-949. doi:10.1080/02786826.2012.683204.
- Lihavainen, H., V.-M. Kerminen, M. Komppula, J. Hatakka, and V. Aaltonen. 2003. Production of "potential" cloud condensation nuclei associated with atmospheric newparticle formation in Northern Finland. J. Geophys. Res. 108 (D24):4782. doi:10.1029/2003JD003887.
- Mutzel, A., L. Poulain, T. Berndt, Y. Iinuma, M. Rodigast, O. Böge, S. Richters, G. Spindler, M. Sipilä, T. Jokinen, et al. 2015. Highly oxidized multifunctional organic compounds observed in tropospheric particles: A field and laboratory study. Environ. Sci. Technol. 49 (13): 7754-7761. doi:10.1021/acs.est.5b00885.

- Newland, M. J., A. R. Rickard, T. Sherwen, M. J. Evans, L. Vereecken, A. Muñoz, M. Ródenas, and W. J. Bloss. 2018. The atmospheric impacts of monoterpene ozonolysis on global stabilised Criegee intermediate budgets and SO2 oxidation: Experiment, theory and modelling. Atmos. Chem. Phys. 18 (8):6095–6120. doi:10.5194/acp-18-6095-2018.
- Paasonen, P., A. Asmi, T. Petäjä, M. K. Kajos, M. Aijälä, H. Junninen, T. Holst, J. P. D. Abbatt, A. Arneth, W. Birmili, et al. 2013. Warming-induced increase in aerosol number concentration likely to moderate climate change. Nat. Geosci. 6 (6):438-442. doi:10.1038/ngeo1800.
- Pathak, R. K., C. O. Stanier, N. M. Donahue, and S. N. Pandis. 2007. Ozonolysis of  $\alpha$ -pinene at atmospherically relevant concentrations: Temperature dependence of aerosol mass fractions (yields). J. Geophys. Res. Atmos. 112:D03201. doi:10.1029/2006JD007436.
- Riccobono, F., S. Schobesberger, C. E. Scott, J. Dommen, I. K. Ortega, L. Rondo, J. Almeida, A. Amorim, F. Bianchi, M. Breitenlechner, et al. 2014. Oxidation products of biogenic emissions contribute to nucleation of atmospheric particles. Science 344 (6185):717-721. doi: 10.1126/science.1243527.
- Riipinen, I., J. R. Pierce, T. Yli-Juuti, T. Nieminen, S. Häkkinen, M. Ehn, H. Junninen, K. Lehtipalo, T. Petäjä, J. Slowik, et al. 2011. Organic condensation: A vital link connecting aerosol formation to cloud condensation nuclei (CCN) concentrations. Atmos. Chem. Phys. 11 (8): 3865–3878. doi:10.5194/acp-11-3865-2011.
- Rissanen, M. P., T. Kurtén, M. Sipilä, J. A. Thornton, J. Kangasluoma, N. Sarnela, H. Junninen, S. Jørgensen, S. Schallhart, M. K. Kajos, et al. 2014. The formation of highly oxidized multifunctional products in the ozonolysis of cyclohexene. J. Am. Chem. Soc. 136 (44): 15596-15606. doi:10.1021/ja507146s.
- Sarnela, N., T. Jokinen, J. Duplissy, C. Yan, T. Nieminen, M. Ehn, S. Schobesberger, M. Heinritzi, S. Ehrhart, K. Lehtipalo, et al. 2018. Measurement-model comparison of stabilized Criegee intermediate and highly oxygenated molecule production in the CLOUD chamber. Atmos. Chem. Phys. 18 (4):2363-2380. doi:10.5194/acp-18-2363-
- Shiraiwa, M., T. Berkemeier, K. A. Schilling-Fahnestock, J. H. Seinfeld, and U. Pöschl. 2014. Molecular corridors and kinetic regimes in the multiphase chemical evolution of secondary organic aerosol. Atmos. Chem. Phys. 14 (16):8323-8341. doi:10.5194/acp-14-8323-2014.
- Tröstl, J., W. K. Chuang, H. Gordon, M. Heinritzi, C. Yan, U. Molteni, L. Ahlm, C. Frege, F. Bianchi, R. Wagner, et al. 2016. The role of low-volatility organic compounds in initial particle growth in the atmosphere. Nature 533 (7604):527-531. doi:10.1038/nature18271.
- Tu, P., W. A. Hall, and M. V. Johnston. 2016. Characterization of highly oxidized molecules in fresh and aged biogenic secondary organic aerosol. Anal. Chem. 88 (8):4495-4501. doi:10.1021/acs.analchem.6b00378.
- Zhang, X., A. T. Lambe, M. A. Upshur, W. A. Brooks, A. Gray Bé, R. J. Thomson, F. M. Geiger, J. D. Surratt, Z. Zhang, A. Gold, et al. 2017. Highly oxygenated multifunctional compounds in α-Pinene secondary organic aerosol. Environ. Sci. Technol. 51 (11):5932-5940. doi: 10.1021/acs.est.6b06588.